

October 25, 2019

Open charm Spectroscopy and exotic states at LHCb

ANTIMO PALANO¹*INFN and University of Bari, Italy*

We present a summary of new experimental results on the status of the charm spectroscopy using inclusive approaches and Dalitz plot analyses of B and B_s decays. We also report on a new determination of the $X(3872)$ quantum numbers.

PRESENTED AT

The 7th International Workshop on Charm Physics
(CHARM 2015)
Detroit, MI, 18-22 May, 2015

¹on behalf of the LHCb Collaboration.

1 Introduction: Charm meson spectroscopy

The quark model predicts many states with different quantum numbers in limited mass regions [1, 2]. New progress in the understanding of the D_J and D_{sJ} spectra in LHCb experiment come from:

- Inclusive studies: study of the reactions $pp \rightarrow D_J/D_{sJ}X$;
- Exclusive studies in Dalitz plot analyses of B and B_s decays.

In the following, we remind that states having $J^P = 0^+, 1^-, 2^+, 3^-, \dots$ are defined as having “Natural Parity”, while states having $J^P = 0^-, 1^+, 2^-, \dots$ are defined as having “Unnatural Parity”. A resonance decaying to $D\pi$ has “Natural Parity”. Labeled with D^* . The $D^*(\pi/K)$ system can access to both “Natural Parity” and “Unnatural Parity” states, except for $J^P = 0^+$ which is forbidden.

In the following, inclusive studies make use of 1 fb^{-1} while Dalitz analyses of 3 fb^{-1} integrated luminosities.

2 Results on D_J mesons spectroscopy

2.1 Inclusive studies

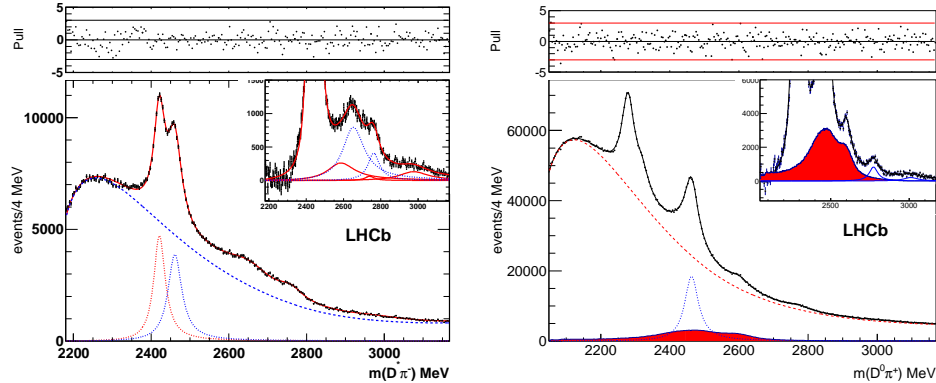


Figure 1: Left: $D^{*+}\pi^-$ mass spectrum with enhanced natural parity selections. Right: $D^0\pi^+$ mass spectrum. Note the crossfeed (in red) from the high mass D_J resonances into the $D\pi$ mass spectra.

The BaBar [3] and LHCb [4] experiments observe two new natural parity resonances, $D^*(2650)$ and $D^*(2760)$, both decaying to $D\pi$ and $D^*\pi$. While the parameters of the $D^*(2760)$ are consistent within the two experiments, the mass of the $D^*(2650)$ state is shifted down by $\approx 40 \text{ MeV}$ in the BaBar analysis due to different handling

of the $D^*\pi$ feedthrough into the $D\pi$ final states. The two states are candidates for being the $J^P = 1^- D_1^3(2S)$ and $J^P = 1^- D_1^3(1D)$.

Adding statistical and systematic uncertainties in quadrature, we obtain a weighted mean values for $D_J^*(2770)$ parameters.

$$m(D_J^*(2770)) = 2768.8 \pm 1.7 \text{ MeV}, \quad \Gamma(D_J^*(2770)) = 63.2 \pm 5.3 \text{ MeV}$$

The $D^{*+}\pi^-$ angular distributions in terms of the helicity angle for the $D_J^*(2650)$ and $D^*(2760)$ are shown in fig. 2. They are well fitted by the $\sin^2\theta_H$ functions and therefore are consistent with having natural parity. LHCb experiment also observes

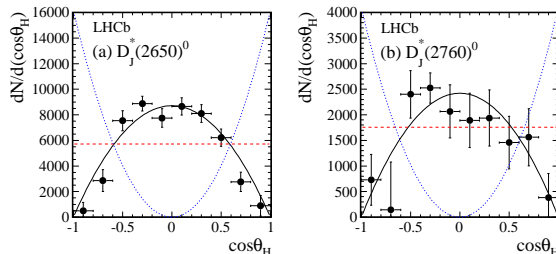


Figure 2: Angular distributions in terms of the helicity angle for the $D_J^*(2650)$ and $D^*(2760)$.

three unnatural parity states, $D_J(2580)^0$, $D_J(2740)^0$, and $D_J(3000)^0$, whose angular distributions are shown in fig. 3. The weighted mean values for $D_J(2580)$ parameters,

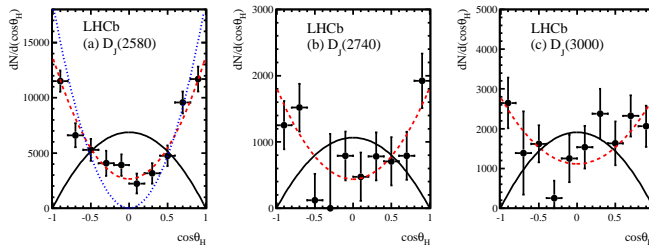


Figure 3: Angular distributions in terms of the helicity angle for the $D_J(2580)^0$, $D_J(2740)^0$, and $D_J(3000)^0$.

consistent with a $J^P = 0^-$ assignment, are

$$m(D_J(2580)) = 2564.0 \pm 5.1 \text{ MeV}, \quad \Gamma(D_J(2580)) = 135.6 \pm 16.9 \text{ MeV}$$

The weighted mean values for the $D_J(2740)$ parameters are

$$m(D_J(2740)) = 2751.3 \pm 3.1 \text{ MeV}, \quad \Gamma(D_J(2740)) = 71.4 \pm 11.4 \text{ MeV}$$

and is a candidate for being a $J^P = 2^-$ state. The broad structures observed in the 3000 MeV mass region could be a superposition of several states.

2.2 First observation and Dalitz plot analysis of $B^- \rightarrow D^+ K^- \pi^-$

The $D^+ K^- \pi^-$ mass spectrum [5] is shown in fig. 4 (Left) and contains $\approx 2K$ events in the B^- signal region. To obtain a high B^- signal purity we make use of neural

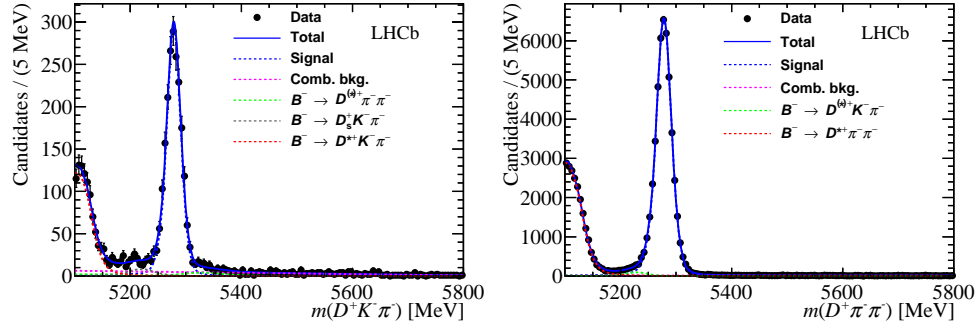


Figure 4: Left: $D^+ K^- \pi^-$ mass spectrum. Right: $B^- \rightarrow D^+ \pi^- \pi^-$ mass spectrum.

network's trained by control samples, especially the $B^- \rightarrow D^+ \pi^- \pi^-$ final state which contains $\approx 49K$ events and shown in fig. 4 (Right). We perform a standard Dalitz plot analysis of the $B^- \rightarrow D^+ K^- \pi^-$ system. In this final state, resonance production can only occur in the $D^+ \pi^-$ system. We plot, in fig. 5, the efficiency corrected and background subtracted $D^+ \pi^-$ mass spectrum, weighted by Legendre polynomial moments and compare with Dalitz plot fit results. We note that P_1 is related to the

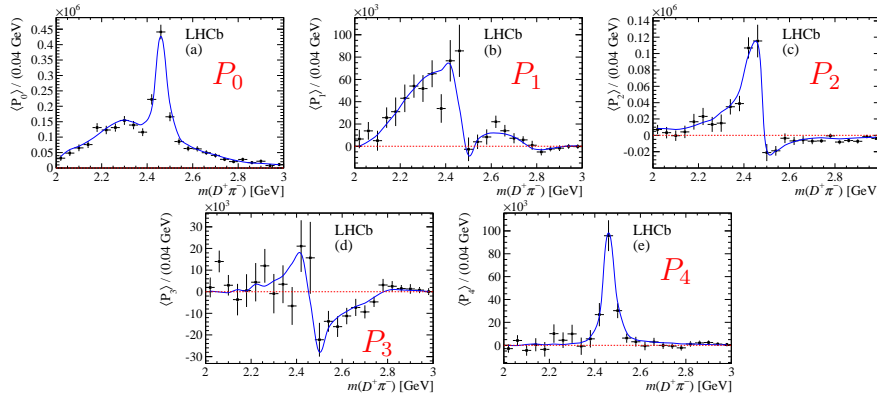


Figure 5: $B^- \rightarrow D^+ K^- \pi^-$. $D^+ \pi^-$ mass spectrum, weighted by Legendre polynomial moments.

S-P interference, while P_3 is related to the P-D interference. We also observe, as expected, a Clear D-wave in P_4 due to the $D_2^*(2460)^0$. In the Dalitz analysis a better fit is obtained introducing virtual $D_v^*(2007)^0$, B_v^{*0} and nonresonant contributions. We also observe a clear spin-2 $D_2^*(2460)^0$ signal and a $D_2^*(2760)^0$ spin-1 resonance. The

Resonance	Spin	Parameters	Fit fraction
$D_0^*(2400)^0$	0	PDG	$8.3 \pm 2.6 \pm 0.6 \pm 1.9$
$D_2^*(2460)^0$	2	$m = 2464.0 \pm 1.4, \Gamma = 43.8 \pm 2.9 \text{ MeV}$	$31.8 \pm 1.5 \pm 0.9 \pm 1.4$
$D_J^*(2760)^0$	1	$m = 2781 \pm 18, \Gamma = 177 \pm 32 \text{ MeV}$	$4.9 \pm 1.2 \pm 0.3 \pm 0.9$

Table 1: $B^- \rightarrow D^+ K^- \pi^-$. Resonances parameters from the Dalitz analysis.

resulting resonance parameters and fitted fractions are given in Table 1. The $D^+ \pi^-$ fit projection with fit result is shown in Fig. 6. No evidence for a $D_3^*(2760)$ spin-3

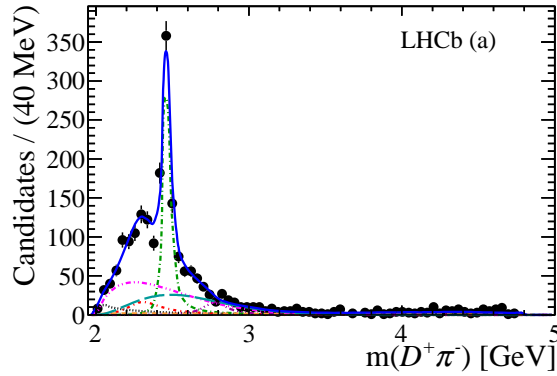


Figure 6: $B^- \rightarrow D^+ K^- \pi^-$. $D^+ \pi^-$ fit projection with fit result.

resonance is found in this final state.

2.3 Dalitz plot analysis of $B^0 \rightarrow \bar{D}^0 \pi^+ \pi^-$

The $\bar{D}^0 \pi^+ \pi^-$ mass spectrum is shown in Fig. 7 (Left) [6]. The B^0 signal contains 9565 events with 97.8% purity. The $B^0 \rightarrow \bar{D}^0 \pi^+ \pi^-$ Dalitz plot is shown in Fig. 7 (Right). We observe the spin-2 $D_2^*(2460)^-$ signal along the $\bar{D}^0 \pi^-$ axis and the spin-1 $\rho(770)$ signal along the $\pi^+ \pi^-$ axis. The Dalitz plot analysis has been performed using the isobar model and a K-matrix description of the $\pi^+ \pi^-$ S-wave. Both methods give a good description of the data. The $m^2(\pi^+ \pi^-)$ fit projection are shown in Fig. 8. We observe a signal of ρ/ω interference. The $m^2(\bar{D}^0 \pi^-)$ fit projection is shown in Fig. 9. The decay is dominated, in the $\pi^+ \pi^-$ system, by S-wave ($16.51 \pm 0.70 \pm 1.68 \pm 1.10$)% and $\rho(770)$ ($36.15 \pm 1.00 \pm 2.13 \pm 0.79$)%. In the $\bar{D}^0 \pi^-$ system, the largest contribution comes from the $D_2^*(2460)^-$ resonance ($28.13 \pm 0.72 \pm 1.06 \pm 0.54$)%.

The Dalitz plot analysis requires the presence of an additional $J^P = 3^-$ resonance with a K-matrix model fitted fraction of ($1.58 \pm 0.22 \pm 0.18 \pm 0.07$)%. The fitted resonances parameters are given in Table 2.

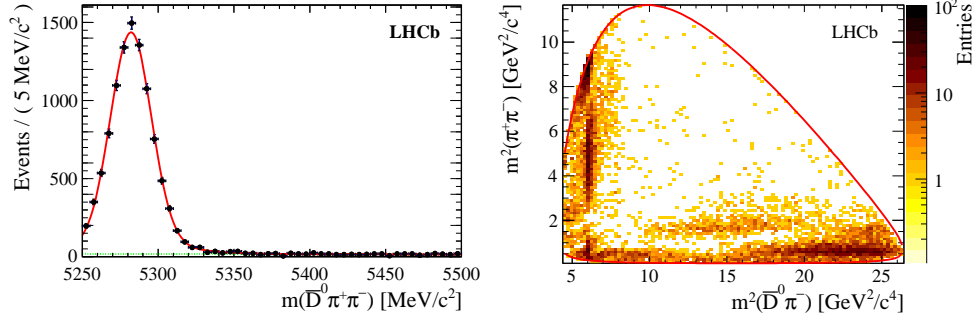


Figure 7: Left: $\overline{D}^0 \pi^+ \pi^-$ mass spectrum. The green line represents the background contribution. Right: $B^0 \rightarrow \overline{D}^0 \pi^+ \pi^-$ Dalitz plot.

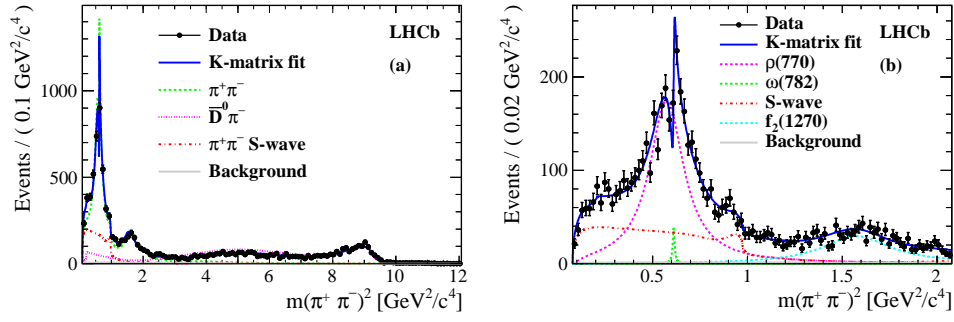


Figure 8: $B^0 \rightarrow \overline{D}^0 \pi^+ \pi^-$. $m^2(\pi^+ \pi^-)$ fit projection with two different binnings.

Comparing the $D_j^*(2760)$ parameters between inclusive and B decays production, we observe some disagreement. Both $J^P = 1^-$ and $J^P = 3^-$ resonances are expected in this mass region and inclusive data cannot separate the two natural parity contributions.

2.4 Dalitz plot analysis of $B^0 \rightarrow \overline{D}^0 K^+ \pi^-$

The $\overline{D}^0 K^+ \pi^-$ mass spectrum is shown in Fig. 10(Left) [7]. The B^0 signal region contains 2344 events. The fit projections are shown in Fig. 11. The decay is dominated by intermediate resonance production of $K^*(892)^0$ ($37.4 \pm 1.5\%$), $D_0^*(2400)^-$ ($19.3 \pm 2.8\%$) and $D_2^*(2460)^-$ ($23.1 \pm 1.2\%$). These Dalitz analyses obtain new parameters for the broad $D_0^*(2400)^-$ resonance which are summarized in Table 3. No evidence is found for additional spin-1 or spin-3 D_j^* resonances.

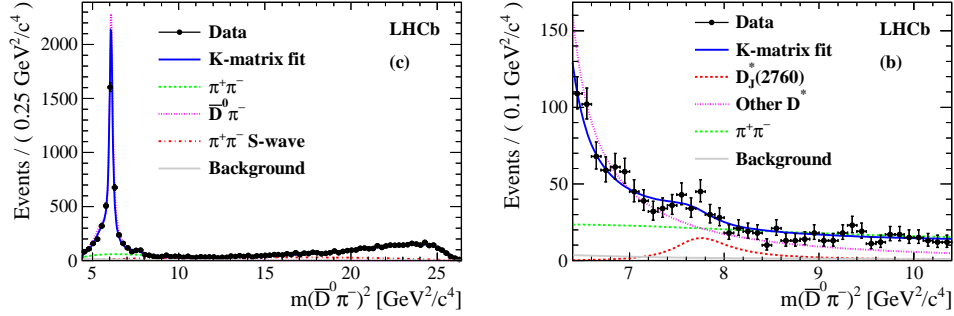


Figure 9: $B^0 \rightarrow \bar{D}^0 \pi^+ \pi^-$. $m^2(\bar{D}^0 \pi^-)$ fit projection with two different binnings.

		Isobar			K-matrix		
$D_0^*(2400)$	m	$2349 \pm 6 \pm 1 \pm 4$			$2354 \pm 7 \pm 11 \pm 2$		
	Γ	$217 \pm 13 \pm 5 \pm 12$			$230 \pm 15 \pm 18 \pm 11$		
$D_2^*(2460)$	m	$2468.6 \pm 0.6 \pm 0.0 \pm 0.3$			$2468.1 \pm 0.6 \pm 0.4 \pm 0.3$		
	Γ	$47.3 \pm 1.5 \pm 0.3 \pm 0.6$			$46.0 \pm 1.4 \pm 1.7 \pm 0.4$		
$D_3^*(2760)$	m	$2798 \pm 7 \pm 1 \pm 7$			$2802 \pm 11 \pm 10 \pm 3$		
	Γ	$105 \pm 18 \pm 6 \pm 23$			$154 \pm 27 \pm 13 \pm 9$		

Table 2: $B^0 \rightarrow \bar{D}^0 \pi^+ \pi^-$. Resonances parameters from the Dalitz analysis.

Final state	Method	Mass	Width
$B^0 \rightarrow \bar{D}^0 K^+ \pi^-$	Free	2360 ± 15	255 ± 26
$B^0 \rightarrow \bar{D}^0 \pi^+ \pi^-$	Free	2354 ± 7	230 ± 15
$B^- \rightarrow D^+ K^- \pi^-$	(PDG)	2318 ± 29	267 ± 40

Table 3: $D_0^*(2400)$ resonances parameters from the different Dalitz analyses.

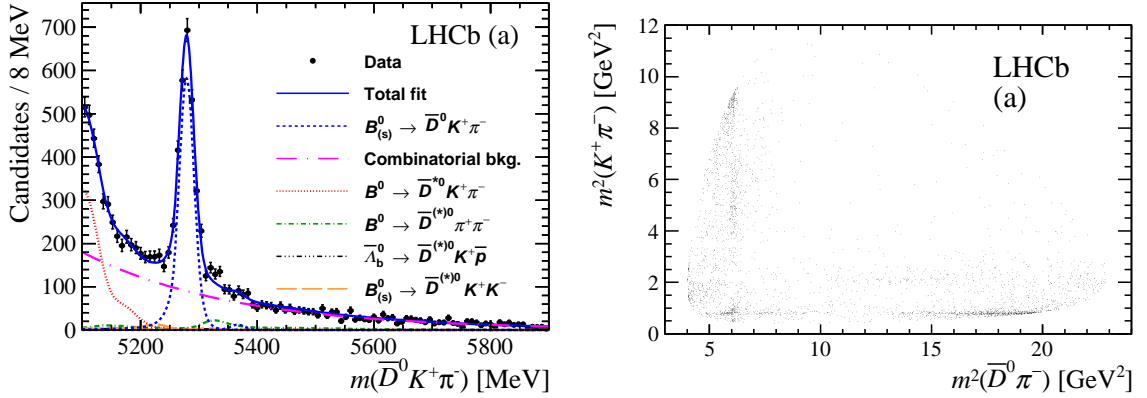


Figure 10: Left: $\bar{D}^0 K^+ \pi^-$ mass spectrum. Right: $B^0 \rightarrow \bar{D}^0 K^+ \pi^-$ Dalitz plot.

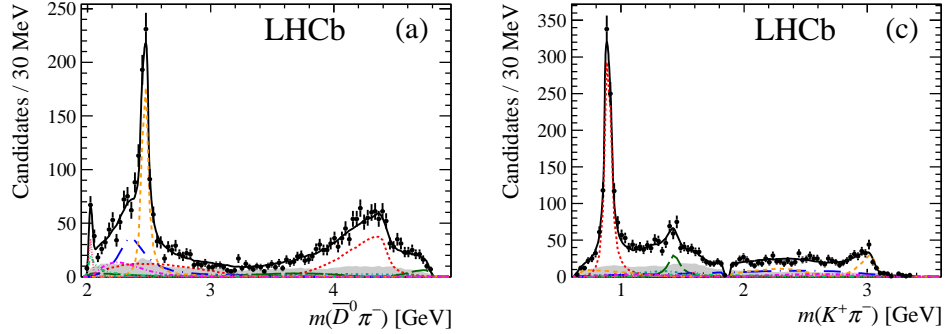


Figure 11: $B^0 \rightarrow \bar{D}^0 K^+ \pi^-$. $m(\bar{D}^0 \pi^-)$ and $m(K^+ \pi^-)$ fit projections.

3 Results on D_{sJ} mesons spectroscopy

3.1 Inclusive studies

Using samples of 0.36×10^6 $D^+ K_s^0$ and 3.15×10^6 $D^0 K^+$ inclusive candidates, the $D_{s1}^*(2710)^+$ and $D_{sJ}^*(2860)^+$ have been observed with parameters consistent with previous measurements [8]. The background subtracted $D^+ K_s^0$ and $D^0 K^+$ mass spectra are shown in Fig. 12.

3.2 Dalitz plot analysis of $B_s^0 \rightarrow \bar{D}^0 K^- \pi^+$

Fig. 13(Left) shows the $\bar{D}^0 K^- \pi^+$ mass spectrum [9]. The B_s^0 signal contains 11302 ± 159 signal events. The Dalitz analysis shows that the largest components are: $\bar{K}^*(892)^0$ (28.6%), $D_{s2}^*(2573)^-$ (25.7%), $K\pi$ S-wave (LASS) (21.4%) $\bar{D}^0 K^-$ nonresonant (12.4%). A signal present in the 2860 MeV $\bar{D}^0 K^-$ mass region which is described by a superposition of a spin-1 ($5.0 \pm 1.2 \pm 0.7 \pm 3.3$)% and a spin-3 ($2.2 \pm 0.1 \pm 0.3 \pm 0.4$)%

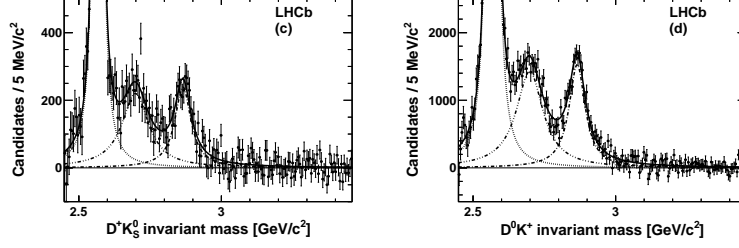


Figure 12: Background subtracted (c) $D^+K_s^0$ and (d) D^0K^+ mass spectra.

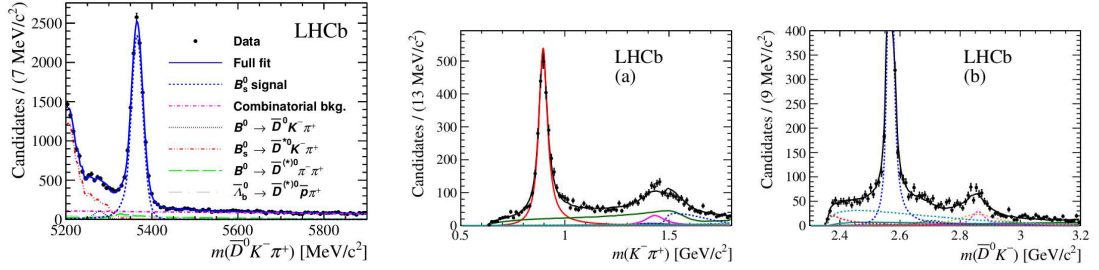


Figure 13: (Left) $\overline{D}^0K^-\pi^+$ mass spectrum. (Right) $K^-\pi^+$ and \overline{D}^0K^- mass projections.

resonance. The fitted resonances parameters are: $m(D_{s1}^*(2860)^-) = 2859 \pm 12 \pm 6 \pm 23 \text{ MeV}/c^2$, $\Gamma(D_{s1}^*(2860)^-) = 159 \pm 23 \pm 27 \pm 72 \text{ MeV}/c^2$, $m(D_{s3}^*(2860)^-) = 2860.5 \pm 2.6 \pm 2.5 \pm 6.0 \text{ MeV}/c^2$, $\Gamma(D_{s3}^*(2860)^-) = 53 \pm 7 \pm 4 \pm 6 \text{ MeV}/c^2$.

3.3 Determination of the $X(3872) \rightarrow J/\psi\rho(770)$ quantum numbers

We study the decay $B^+ \rightarrow X(3872)K^+$ with $X(3872) \rightarrow J/\psi\pi^+\pi^-$ [10] [10]. The quantum numbers of $X(3872) \rightarrow J/\psi\rho(770)$ have been determined to be $J^{PC} = 1^{++}$. However it was assumed that the decay is dominated by the lowest values of angular momentum between the $X(3872)$ decay products. The analysis is repeated here using 3-times the statistics and without any assumption on L_{min} . The ΔM signal for $J/\psi\pi^+\pi^-$ is shown in Fig. 14. The B^+ signal for $B^+ \rightarrow X(3872)K^+$ contains 1011 ± 38 with 80% signal purity.

The distributions of the test statistic $t \equiv -2 \ln[\mathcal{L}(J_X^{\text{alt}})/\mathcal{L}(1^{++})]$, for the simulated experiments under the $J^{PC} = J_X^{\text{alt}}$ hypothesis and under the $J^{PC} = 1^{++}$ hypothesis are shown in Fig. 14 The $J^{PC} = 1^{++}$ hypothesis gives the highest Likelihood value with an upper limit of D -wave contribution of 4% at 95% C.L.

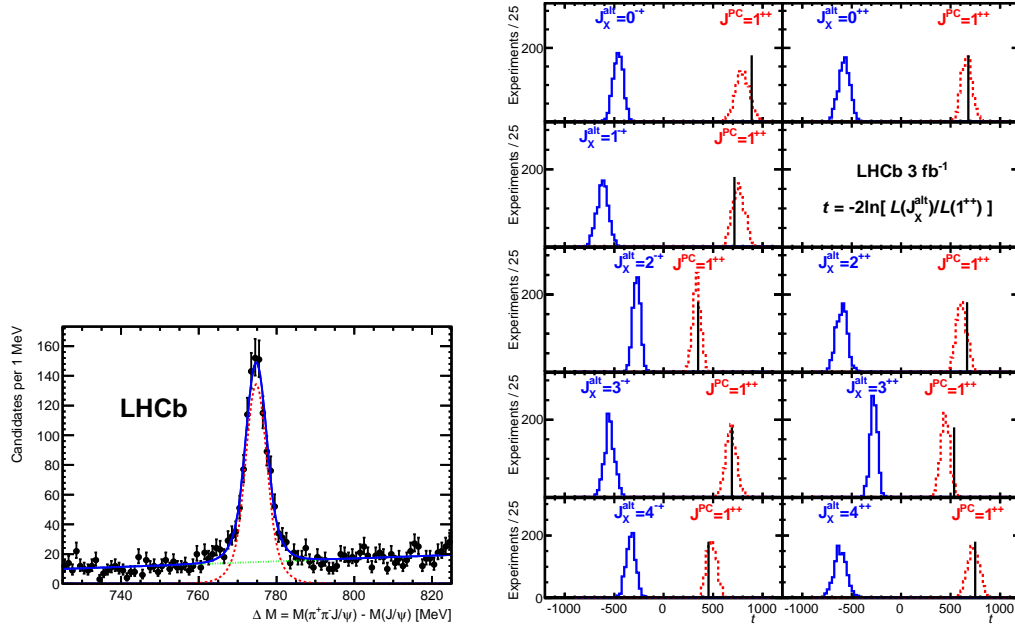


Figure 14: (Left) X(3872) signal. (Right) Distributions of the test statistic for different spin-parity hypothesis.

References

- [1] Godfrey and Isgur, Phys.Rev. **D32**,189 (1985).
- [2] S. Godfrey and I. T. Jardine, Phys. Rev. **D89**, 074023 (2014).
- [3] BaBar collaboration, P. del Amo Sanchez, P. *et al.*, Phys. Rev. **D82**, 111101 (2010).
- [4] LHCb collaboration, R. Aaij *et al.*, JHEP **09**, 145 (2013).
- [5] LHCb collaboration, R. Aaij *et al.*, Phys. Rev. **D91**, 092002 (2015).
- [6] LHCb collaboration, R. Aaij *et al.*, Phys. Rev. **D92**, 032002 (2015).
- [7] LHCb collaboration, R. Aaij *et al.*, Phys. Rev. **D92**, 032002 (2015).
- [8] LHCb collaboration, R. Aaij *et al.*, JHEP **1210**, 151 (2012).
- [9] LHCb collaboration, R. Aaij *et al.*, Phys. Rev. **D 90**, 072003 (2014).
- [10] LHCb collaboration, R. Aaij *et al.*, Phys.Rev. bf D92, 011102 (2015)